Astron. Astrophys. 338, 995–1005 (1998)

ASTRONOMY AND ASTROPHYSICS

Gas and grain chemistry in a protoplanetary disk

K. Willacy[1⋆], H.H. Klahr[2], T.J. Millar[1], and Th. Henning[2]

[1] Department of Physics, UMIST, P.O. Box 88, Manchester, England, UK
[2] Astrophysical Institute and University Observatory, Schillergässchen 3, D-07745 Jena, Germany

Received 21 April 1998 / Accepted 29 July 1998

Abstract. The chemistry in a protoplanetary accretion disk is modelled between a radius of 100 and 0.1 AU of the central object. We find that interaction of the gas with the dust grains is very important, both by removing a large fraction of the material from the gas in the outer regions and through the chemical reactions which can occur on the dust grain surfaces. In addition, collision with grains neutralises gaseous ions effectively and keeps the ionization fraction low. This results in a chemistry which is dominated by neutral–neutral reactions, even if ionization is provided by cosmic rays or by the decay of radioactive isotopes. We model the effects of two desorption processes with very different efficiencies and find that while these produce similar results over much of the disk for many species, some molecules are extremely sensitive to the nature of the desorption and may one day be used as an observational test for the desorption process.

Key words: stars: formation – stars: pre–main sequence – accretion, accretion disks – molecular processes – dust, extinction

1. Introduction

When a molecular cloud collapses it can form a protostar at its centre. Models of this process predict that conservation of angular momentum will lead to the creation of a flattened accretion disk surrounding the protostar (cf. Bodenheimer 1995). Material in the disk is transported radially inwards with angular momentum being viscously transported outwards. It is likely that planets and other bodies are formed in the disk and for this reason interest in the chemistry and physics of the disk is growing. One aim of this type of research is an understanding of the conditions in the pre–solar nebula and how they led to the formation of our own Solar System.

Observations of the T–Tauri stars have confirmed the presence of accretion disks and suggest that they are relatively common (see for example Beckwith & Sargent 1993, Strom et al. 1993). Although the available instrumentation does not have the resolution necessary to probe the innermost parts of the disk or to investigate the chemistry in detail, some progress is being made. Recently Dutrey et al. (1997) have detected emission from CO, CN, HCN, HNC, CS, HCO^+, C_2H and H_2CO in the disks surrounding DM Tau and GG Tau. These measurements are single dish and are not sensitive to the inner 100 AU of the disk. In common with other studies (e.g. interferometric observations of CS in HL Tau by Blake et al. 1992) they find that the molecules are underabundant by factors of between 5 (for CO) and 100 (for H_2CO) compared with those in molecular cloud cores such as TMC–1. This combined with the results of chemical modelling of dense regions, e.g. Bergin & Langer (1997), suggests the depletion of molecules by freezeout onto dust grains.

Some work has been done on modelling the chemistry in protoplanetary disks. Aikawa et al. (1997) considered the time–dependent chemistry of a disk at two points where the temperature is 30 and 90 K. They included cosmic ray ionization, freeze-out onto grains and thermal desorption but no mantle chemistry. They found that cosmic rays are important, forming ions which destroy CO and N_2, causing depletion of these molecules in the gas phase. In the solid phase they find that oxidized ice (CO_2) and reduced ice (e.g. NH_3) can coexist. This coexistence is also a characteristic of comets (Yamamoto 1991). Another important prediction of this model is that the molecular abundance in the gas and in the ice mantle varies considerably with distance from the central star.

The Heidelberg group have considered the chemical composition of a parcel of gas as it is transported inwards towards the centre of the disk (e.g. Bauer et al. 1997, Duschl et al. 1996). They have mainly concentrated on the region in the centre of the disk where the dust is destroyed, although their model does cover the region from 1000 AU inwards. All elements not incorporated into the dust are in H, H_2, CO, H_2O and N_2 with the CO and H_2O forming icy mantles. This limitation in the initial conditions affects the chemistry which can proceed in the outer disk and chemistry only really starts to occur in their model when the dust is destroyed. The outer disk just reflects the initial conditions. In the region of dust destruction they find a complex chemistry occurring, with the carbonaceous grains being processed into simple hydrocarbons (CH_n) and then into CO and the oxygen released by the silicate evaporation form-

Send offprint requests to: K. Willacy

⋆ *Present address:* Jet Propulsion Laboratory, California Institute of Technology, MS 169–327, Pasadena CA 91109

ing H_2O. Most molecules dissociate at radii less than 0.06 AU, where the temperature is greater than 2000 K, with H_2 dissociating at $R < 0.05$ AU. Hence in the innermost part of the disk only free atoms exist.

In this paper we consider the chemistry in the region of the disk between 100 AU and 0.1 AU (in our model the point at which the temperature is sufficiently high that dust destruction will begin). We consider the gas–grain interactions – freezeout, desorption and grain mantle chemistry, together with a description of the gas phase chemistry. In the next section we describe the physical and chemical models and the desorption and other processes included. We discuss the results and compare them with other models of accretion disks.

2. The model

2.1. Dynamical model

Before calculating the chemistry one must know the density and temperature distribution typical for a protoplanetary nebula. We determined the vertical and radial structure of a given viscously heated disk by calculating a radial series of one–dimensional vertical structure integrations (Bell et al. 1997). The mass flux $\dot{M}$, the viscous efficiency α, (Shakura & Sunyaev 1973) and stellar mass $M_\star$, are taken to be constant (in time and space) for a given model. Axial symmetry is assumed.

As long as the disk is geometrically thin one can neglect the radial diffusion of energy and a one-dimensional approximation is sufficient (Pringle 1981). Then the dissipated energy is radiated locally (i.e. vertical transport of energy to the surfaces of the disk predominates over radial transport) and the internally produced accretion flux ensues for the radiation temperature $T_{\rm acc}$ at the surface of the disk $H_R = z$:

$$\sigma T_{\rm acc}^4 = \frac{3GM_\star\dot{M}}{8\pi r^3}\left(1-\sqrt{\frac{R_\star}{r}}\right) \quad (1)$$

with the Stefan-Boltzmann constant σ, the gravitational constant G and the radius of the central object (the star) $R_\star$. The variables r and z are the radial and vertical coordinates. The fundamental equations for the vertical integration are (cf. Meyer & Meyer-Hofmeister (1981, 1982)

$$\partial_{\rm z}P = -g_{\rm z}\rho = -\frac{\rho\, GM_\star z}{(r^2+z^2)^{3/2}} \quad (2)$$

$$\partial_{\rm z}T = -\frac{\tilde{\kappa}\rho F}{4ac\lambda T^3} \ \text{ if } \ \nabla_{\rm rad} \le \nabla_{\rm ad} \quad (3)$$

$$\partial_{\rm z}T = g_{\rm z}\rho\frac{T}{P}\nabla_{\rm conv} \ \text{ if } \ \nabla_{\rm rad} > \nabla_{\rm ad} \quad (4)$$

$$\partial_{\rm z}F = \frac{9}{4}\frac{GM_\star\rho\nu}{r^3} \quad (5)$$

where P, T, ρ and F are respectively, pressure, temperature, density and radiation flux. Further quantities are the Rosseland mean opacity $\tilde{\kappa}$ (given by $\tilde{\kappa} = \tilde{\kappa}_n\rho^{\alpha_n}T^{\beta_n}$ using analytical formulae by Bell & Lin (1994) and Henning & Stognienko (1996)), the radiation constant a, speed of light c, a fluxlimiter λ, (see Levermore & Pomraning (1981)) and the kinematic viscosity ν, (given by $\nu = \alpha c_s^2/\Omega$, with the isothermal sound-speed c_s, and the Keplerian frequency Ω). The nabla operators are defined according to Kippenhahn et al. (1967).

The vertical integration starts at the optical depth $\tau = 2/3$ at height H_R with the surface temperature, T_{acc}, due to locally generated energy from Eq. (1). The density at the surface is found from the assumption of pressure balance. Starting from a guess of the photospheric thickness, H_R, Eqs. (2) to (5) are integrated over z down to the mid-plane of the accretion disk, $z = 0$. The photospheric thickness is repeatedly modified until a solution is found in which the radiative flux vanishes in the mid-plane, $F(z = 0) = 0$. Full details of this calculation are given in Bell & Lin (1994). The results of this 1D-vertical calculation agree very well to the density and temperature distributions obtained by 2D-hydrodynamical calculations (Różyczka et al. 1994). Analytical "two-zone" models, used by other groups, neglect the vertical variation of the opacity and viscosity, and the effects of convective energy transport, thus leading to a simplified temperature and density distribution.

For our standard protoplanetary accretion disk we assumed the following parameters $\alpha = 0.01$, $\dot{M} = 10^{-7}{\rm M}_\odot{\rm a}^{-1}$, and $M_\star = 1{\rm M}_\odot$. The resulting density and temperature structure are shown in Fig. 1a and b.

Although our density structure is very similar to that of Finocchi et al. (1997), we find considerable differences in the temperature distribution (see Fig. 1b). Our temperature at small radii is much lower than theirs resulting in dust destruction occurring much closer to the central protostellar object. The difference in temperature structure appears to arise from our use of a higher viscosity. At the same accretion rate this leads to a lower surface density and therefore a lower temperature.

2.2. Chemical model

We have considered the time–dependent chemistry in a 1–dimensional protoplanetary disk. The chemistry has been considered separately from the dynamics since it has little effect on the dynamical model (Bauer et al. 1997). The physical parameters at each radii are assumed to be constant with time. The chemistry is followed at several radii ranging between 100 and 0.1 AU, using the output abundances from one radius as the input to the next smallest radius. The chemical input at 100 AU assumes that all the elements are in their atomic form except for hydrogen which is 99% molecular and carbon which is ionic. The effect of varying the initial abundances is discussed in Sect. 3.8. We have taken 10% of the diffusive timescale at each radius as an indication of the time over which the chemistry can proceed without the physical parameters changing greatly i.e. the time before the gas has moved sufficiently far for the physical parameters to have changed significantly. Although we follow the full time–dependence of the chemical evolution, we find that in general a quasi–steady state is achieved before this time is reached, with the abundances only changing extremely slowly for some time after this point (see Fig. 6). Allowing the chemistry to proceed indefinitely can alter the abundances considerably and this is discussed in Sect. 3.7.

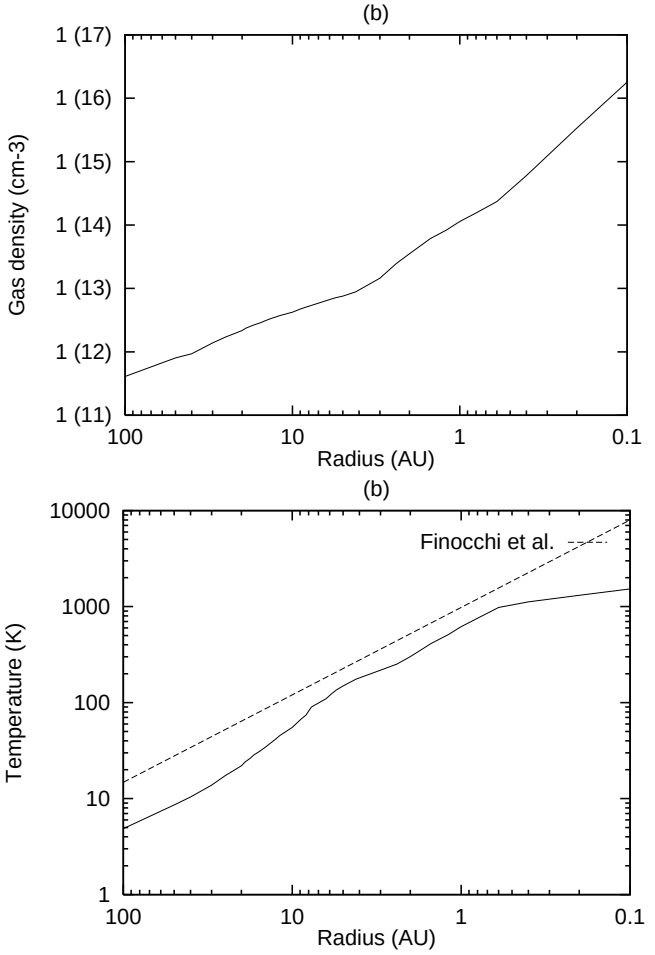

Fig. 1a and b. The physical conditions in the disk used in this work. **a** is the density profile and **b** is the temperature profile. The dotted line in **b** shows the temperature used in Finocchi et al. (1997).

The gas phase chemistry is taken from the current version of the UMIST ratefile (Millar et al. 1997) with additional neutral–neutral reactions taken from the NIST database (Mallard et al. 1994). Our species set consists of a total of 241 species (174 gaseous and 69 solid) made up of the elements H, He, C, N, O, S, Si, Fe and Mg. The reaction network which links them comprises 2055 gaseous two–body reactions, 335 gas–grain interaction processes, 106 grain surface reactions and 144 three–body/collisional dissociation reactions.

2.3. Three body reactions

Since the density of the inner regions of the disk is high ($n > 10^{14}$ cm^{-3}), we have included three–body and collisional dissociation reactions for all neutral species. The rates for these are given in Appendix A. Where published data are not available the collisional dissociation rates have been estimated as

$$k_{cd} = 10^{-10} exp(-E_{bond}/T) \quad \mathrm{cm^3 s^{-1}} \tag{6}$$

where E_{bond} is the energy of the bond which is to be broken and T is the temperature of the gas. A few of the rates for the three–body association reactions are given in Kerr & Moss (1981), Baulch et al. (1982) and Bahn (1968). The others are calculated from the thermodynamics of the reaction using

$$k_{3b} = AT^n C^{\Delta\nu} exp\left\{\frac{\Delta G_R - E_\alpha}{RT}\right\} \quad \mathrm{cm^6 s^{-1}} \tag{7}$$

where A, n and E_α are the Arrhenius parameters for the forward (collisional dissociation) reaction, $C = N \times 10^6/RT$ is the conversion factor from atmosphere to cm^{-3} units, $\Delta\nu$ is the stochiometric factor, N is Avogadros number and R is the ideal gas constant. ΔG_R is the Gibbs free energy of the forward reaction at a gas pressure of 1 atmosphere. This is calculated from the Gibbs free energies of formation taken from the JANAF thermochemical tables (Chase et al. 1985).

The majority of the measured rates are valid for temperatures greater than 1000 K. Therefore these reactions have only been included in the model in the inner regions of the disk ($R < 1$ AU) where this temperature is reached.

2.4. Ionization reactions

Cosmic rays are the main source of ionization in much of the interstellar medium. However they can only penetrate material up to densities of about 150 gcm^{-2} (Umebayashi & Nakano 1981). Beyond this, ionization can occur through the decay of radioactive isotopes which release energetic particles. ^{26}Al decays by emitting a positron which causes ionization in the same way as cosmic rays – by the collisional ionization of H_2 and He. We have assumed that the decay of ^{26}Al can cause ionization with a rate $\zeta = 6.1 \times 10^{-18}$ s^{-1} (Umebayashi & Nakano 1981) which is 0.47 $\times$ the CR ionization rate. This is an order of magnitude larger than that used by Finocchi et al. (1997) and maximizes the effect of ionization in driving the ion–molecule chemistry.

We do not consider the effects of any UV radiation emitted by the central protostellar object since the disk is assumed to be optically thick.

2.5. Gas–grain interactions

The effects of gas–grain interactions are included in the model. For all radii the grain temperature is assumed to be the same as that of the gas. At low temperatures a gas phase molecule which collides with a grain sticks to it efficiently. The freezeout rate is given by

$$k_f = S_x C < \pi a^2 n_g > v_x n(x) \quad \mathrm{cm^{-3} s^{-1}} \tag{8}$$

where S_x is the sticking coefficient (taken to be 0.3 for all species), a is the grain radius, n_g is the number density of grains, v_x is the velocity of the gas phase species and $n(x)$ is the number density of species, x. C is a factor which takes into account the charge of the accreting particle. For neutral species C = 1. We have assumed that positive ions have an enhanced freezeout rate due to their increased attraction to the grains which are taken to

be negatively charged (Umebayashi & Nakano 1980, Taylor et al. 1991). For ions C is given by

$$C = 1 + \frac{16.71 \times 10^{-4}}{(a/cm)(T/K)} \quad (9)$$

2.5.1. Desorption processes

The cold temperatures at the outer edge of the disk mean that accretion on to grains is efficient. In order to keep molecules in the gas in this region some sort of desorption process must be acting. We have considered 3 processes:-

1. Cosmic ray heating of grains:
   When a cosmic ray passes through a grain it deposits heat, causing desorption along its path (Léger et al. 1985). This process has been modelled in dark clouds by Hasegawa & Herbst (1993) and we have adopted their rates here. This assumes that the desorption rate for a molecule is dependent on its binding energy. Cosmic ray heating of grains will only occur in those regions of the disk where the density of the gas is low enough to allow the cosmic rays to penetrate. Hence the effects of this process are restricted to $R > 10$ AU.
2. Explosions caused by grain–grain collisions:
   Given the high densities in the disk it is possible that grain–grain collisions can also trigger mantle removal. Shalabeia & Greenberg (1994) give the rate at which explosions are induced as a result of this process as

   $$R_{expl} = n_g v_g \sigma_g \quad \mathrm{s}^{-1} \quad (10)$$

   where σ_g is the collisional cross–section of a grain and v_g its velocity. Although the turbulent velocity of the gas is $\sim 10^4$ cms^{-1}, the relative velocity of the grains is much smaller ($\sim$ 1 mms^{-1}) (Ossenkopf 1993). Therefore the collision timescale assuming the standard dust/gas parameters is

   $$\tau_{coll} = \frac{2 \times 10^{14}}{n_H} \quad \text{years} \quad (11)$$

   Hence at 100 AU where the density is 4×10^{11} cm^{-3} the desorption rate is

   $$k_{expl} = 6.34 \times 10^{-11} \quad \mathrm{s}^{-1} \quad (12)$$

   which is about 1000 times higher than the cosmic ray heating rate, but still considerably lower than the freezeout rate at these densities. This process is assumed to remove all molecules at the same rate, regardless of their binding energies.
   A point to note is the requirement of a minimum of 1% concentration of radicals in the mantle in order for this process to act efficiently (Schutte & Greenberg 1991). At high densities the abundance of H–atoms is low and therefore the removal of radicals by hydrogenation on the grain surfaces is not as important as at low densities, possibly leading to a buildup of radicals (see Willacy & Millar 1998 for a discussion). However another consideration is the low level of ionization at high densities and therefore the rate of formation of radicals may also be very low, rendering this desorption process inefficient.
   In this model we have assumed that the necessary concentration of radicals are present and that the rate of desorption is independent of this (as per Schutte & Greenberg 1991). Our results should therefore be considered to represent an upper limit to the effects of explosive desorption – if radicals are unable to build up in sufficient quantities then the desorption will be much less efficient.
3. Thermal desorption:
   In cold dark clouds thermal evaporation of grain mantles is unimportant. However in the protoplanetary disk the temperatures are relatively high and this process dominates grain mantle removal over part of the region considered in our model. In the outer part of the disk ($R > 10$ AU) where the temperature is less than about 30 K, this process is inefficient.
   We have used the binding energies given in Hasegawa & Herbst (1993) except for a few molecules for which the values assumed are given in Table 1.

Table 1. The binding energies for some species used in this model compared to those in Hasegawa & Herbst (1993) (HH93). References are (1) Sandford & Allamandola (1993); (2) Yamamoto et al. (1983).

Species	Binding energy	
	HH93	This work
CH_3OH	2060	4235[1]
NH_3	1100	3075[1]
H_2O	1863	4815[1]
SO_2	3070	3460[1]
CO_2	2500	2860[1]
HCN	1760	4170[2]
N_2	1210	710[2]
C_2H_2	1610	2400[2]
CH_4	1360	1080[2]

The results of two models are presented here. Both include the effects of thermal desorption which will dominate in the central parts of the disk, but one (model CRH) considers cosmic ray heating of grains and the other, (model GR) explosive desorption triggered by grain–grain collisions.

2.6. Dust destruction

Dust grains contain most of the refractory elements such as silicon and iron and a sizeable proportion of the carbon and oxygen. In the innermost regions of the disk the temperature is sufficiently high to begin to destroy the dust grains. The carbonaceous grains sublimate at slightly lower temperatures than the silicates at about 1500K (from Duschl et al. 1996). The temperature estimate is based on the conversion of solid carbon into gaseous carbon chains and their subsequent chemical processing into CO. Duschl et al. (1996) also considered the effects of erosion of the carbon grains by reaction with gaseous molecules and concluded that this would lead to destruction of these grains at temperatures above 900 K. Silicates are more refractory and

survive until the temperature reaches 1500 – 1600 K. In our model this means that the grains would begin to evaporate at $R < 0.11$ AU. If oxidation of the carbon grains occurs they will be destroyed at $R < 0.28$ AU. Thus only the very centre of our model disk is affected. We have therefore ignored the effects of dust evaporation in the work presented in this paper. Future work will consider the destruction of refractory grains.

If dust evaporation were included there would be an increase in the abundance of carbon, oxygen and especially of silicon and iron, either in the atomic form or as part of a molecule e.g. SiO. The effect on the gas phase chemistry has been investigated by Finocchi et al. (1997), Bauer et al. (1997) and Duschl et al. (1996).

3. Results

The high densities in the accretion disk result in high freezeout rates and the heating of grains by cosmic rays in model CRH is not efficient enough to keep molecules in the gas. Molecules are almost completely removed from the gas until the region of the disk where thermal desorption starts to become effective (i.e. at $R \sim 20$ AU where $T \sim 22$ K). The gas phase abundances at smaller radii reflect the grain surface abundances. Molecules reappear in the gas in order of increasing binding energy and they retain the same abundance levels until about 2.5 AU. The more efficient grain–grain collisions in model GR are able to keep a small fraction of some molecules off the grains in the outer part of the disk e.g. CO, CO_2, H_2O, HCN, HNC, O_2, NH_3 and C_3H_4 have fractional abundances between 10^{-10} and 10^{-8} at radii greater than 20 AU. For the majority of species the calculated abundance distributions are not affected by the type of desorption. There are a few exceptions which are discussed below.

For both models the abundances are 'frozen out' over much of the disk, with the gas phase chemistry having little effect. Instead the abundances reflect the chemistry which has occurred in the outer parts of the disk. The ionization level is very low (see Sect. 3.1) so the chemistry is dominated by neutral–neutral reactions which act on timescales longer than the dynamical timescales unless the temperature is greater than about 300 K ($R < 2$ AU).

Collisional dissociation reactions are important at $T > 1000$ K. They remove hydrogen atoms from saturated carbon–chain molecules and break down some molecules e.g. SO_2 into their constituent atoms, allowing the formation of other species. Three–body association reactions are not important at the densities reached in this model but may have a role to play at the still higher densities associated with smaller radii. At small radii the major reaction pathways involve the most abundant species H and H_2.

3.1. The ionization level in the disk

Although cosmic rays can penetrate the outer part of the disk and ^{26}Al provides a similar rate of ionization in the denser parts of the disk, we find that the overall ionization level is low. At about 100 AU the fractional abundance of electrons is about 10^{-13} in model CRH and about a factor of 10 higher in model GR. In CRH the dominant ions are H_3^+ and H^+ and these are also important in model GR but in the latter case there are also some molecular ions present (HCO^+ and H_3O^+) resulting from the higher abundance of gaseous molecules in this model. Moving inwards through the disk the ions which carry the charge change. Once thermal desorption becomes efficient the ionization levels and the carrier ions are the same in both models. CO is one of the first molecules to be desorbed and so at 20 AU HCO^+ is the major ion. On moving further inwards $HCNH^+$ appears and then CH_3CO^+ and NH_4^+ at $R < 10$AU.

If we assume that ions do not freezeout then we see a rise in the ionization level by a factor of 10. The charge is mainly carried by the heavy element ions Fe^+ and Mg^+. These are already present in the gas and are not due to dust grain destruction.

Finocchi et al. (1997) find that the ionization in the outer disk is relatively low (f(e) $\sim 3 \times 10^{-12}$ at $R > 25$ AU). This value is within a factor of 10 of ours, with the difference probably being due to the freezeout of ions which is included in our model but not in Finocchi et al. The ionization level rises slightly to $\sim 10^{-10}$ between 20 and 3 AU but increases sharply at about 1 AU where the silicate dust is destroyed. This releases several heavy elements into the gas e.g. K, Na, Ca, Al, Mg and Fe and the ionization of these by the radioactive decay of ^{26}Al causes a huge increase in the ion population and hence in the importance of the ion–molecule chemistry. Hence the complex chemistry seen at this radius in their model. It is unclear at the moment how much of the ionization would remain if the neutralisation of ions by collision with grains were included.

We now consider the chemistry of some species in detail. Although the figures show the results for the model which includes cosmic ray heating, both they and the discussion pertain equally to the model including explosive desorption unless otherwise stated.

3.2. H and H_2

At all radii the dominant form of hydrogen is the molecular form. However at $R < 10$ AU we find a marked increase in the abundance of the atomic form and this is important for the chemistry. Molecular hydrogen is broken down by reaction with H_2^+ and by destruction by ionization caused by the decay of ^{26}Al.

3.3. Oxygen bearing species

H_2O is formed efficiently on the grains by hydrogenation of oxygen atoms whereas CO is mainly formed in the gas and then accreted. CO_2 exists in a ring between 10 and 2 AU (Fig. 2). It is formed on the grain by

$$\mathrm{O} : gr + \mathrm{HCO} : gr \longrightarrow \mathrm{CO_2} : gr + \mathrm{H} : gr \qquad (13)$$

and evaporated. The possible reaction between solid CO and O forming CO_2 has been excluded from our model due to the

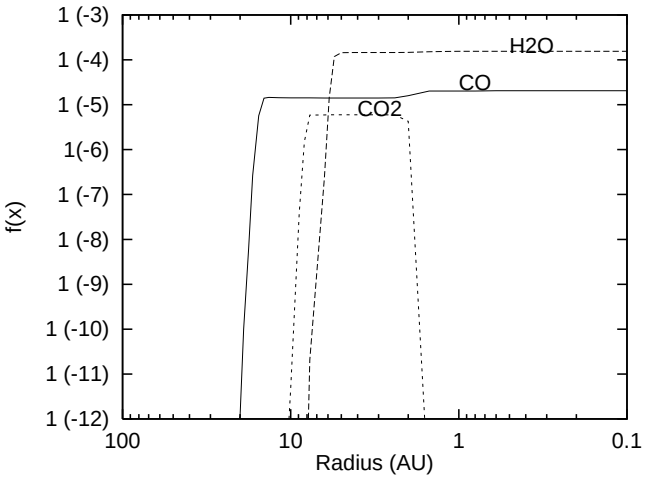

Fig. 2. The variation in the fractional abundance with respect to the total density of CO, CO_2 and H_2O with radius in the CRH model. The reappearance of the molecules in the gas is due to thermal desorption and the difference in the binding energies of the molecules is reflected in the different radii at which this occurs. CO_2 is destroyed at 2 AU by reaction with H_2

uncertainty in its rate. CO_2 is removed from the gas by reaction with H_2

$$CO_2 + H_2 \longrightarrow CO + H_2O \quad (14)$$

This reaction has an activation barrier of 7550 K and therefore CO_2 remains in the gas until $R < 2$ AU where the temperature is greater than 300 K and this reaction begins to occur. The destruction of CO_2 leads to a corresponding increase in the abundance of CO and H_2O.

O_2 and NO are greatly affected by the choice of desorption. In model GR there is a continually, if slow, return of these two molecules to the gas. There they undergo reactions which convert them into other, less reactive, molecules. O_2 is destroyed by

$$O_2 + H^+ \longrightarrow O_2^+ + H \quad (15)$$

$$O_2^+ + e \longrightarrow O + O \quad (16)$$

The oxygen atoms freezeout and form water ice. In the gas H_2 reacts with HCO^+ forming H_3O^+ which in turn reacts with electrons to reform water.

NO reacts with NH:

$$NH + NO \longrightarrow N_2 + O + H \quad (17)$$

Again the oxygen atoms end up in water ice and N_2 also freezes out. The small amount of N_2 which is returned to the gas is cycled to N_2H^+ by reaction with H_3^+ and back to N_2.

3.4. Sulphur–bearing species

In both models SO_2 is the dominant sulphur–bearing species between 100 and 0.4 AU, tying up more than 90% of the available sulphur (Fig. 3). SO_2 is formed on the grains by

$$SO : gr + O : gr \longrightarrow SO_2 : gr \quad (18)$$

H_2CS is the next most abundant species and is also a product of grain surface chemistry

$$HCS : gr + H : gr \longrightarrow H_2CS : gr \quad (19)$$

$$CH_3 : gr + S : gr \longrightarrow H_2CS : gr + H : gr \quad (20)$$

There are no mantle destruction processes for this molecule and it is thermally desorbed at about 11 AU.

C_2S is formed in the gas at 100 AU by

$$S^+ + C_3H \longrightarrow C_3S^+ + H \quad (21)$$

followed by

$$C_3S^+ + e \longrightarrow C_2S + C \quad (22)$$

This process is efficient at early times due to the high abundance of S^+ (which comprises almost all of the sulphur) but the formation rate quickly drops as the sulphur is processed into SO_2 and the ionization level falls. Most of the C_2S is removed from the gas on formation and a large abundance builds up on the grain.

H_2S is not important at $R > 1$ AU in either model. It forms on the grain by hydrogenation of HS but is rapidly destroyed by reaction with H–atoms. In addition the supply of HS is gradually used up as it reacts with oxygen atoms to form SO. Its gas phase production involves the recombination of H_3S^+ with electrons and since the ionization level is low this process is inefficient. Both models show H_2S gradually forming at $R < 1$ AU where

$$S \xrightarrow{H_2} HS \xrightarrow{H_2} H_2S \quad (23)$$

becomes important. The sulphur atoms are supplied by the collisional dissociation of other sulphur bearing molecules, principally SO_2, although the destruction of C_2S is also important. This new supply of sulphur atoms also leads to an increase in H_2CS at small radii by

$$S + CH_3 \longrightarrow H_2CS + H \quad (24)$$

(the CH_3 is produced by collisional dissociation of methane). HS is also produced with some SiS forming in model CRH.

3.5. Carbon–chains

High abundances of some quite large carbon–chain molecules are predicted to form in both models. The chemical reactions schemes end with C_2H_2, C_3H_4 and C_4H_2 and the abundances of these species are therefore likely to be artificially high. However the chemistry as it stands serves to illustrate the kinds of processes which are acting and the types of molecules which could form in a protoplanetary disk. Future work will extend the carbon–chain chemical network and investigate this further. In both models grain surface reactions are responsible for the production of a large proportion of the carbon–chain molecules. Since hydrogenation is so efficient it seems likely that extending the chemistry will result in saturated molecules, leading to the presence of long chain saturated molecules e.g. C_2H_6 in the outer ($R > 1$ AU) part of the disk.

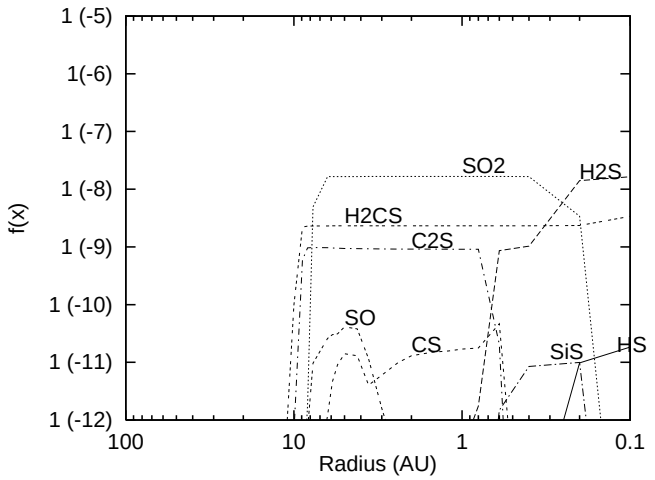

Fig. 3. The radial distribution of the fractional abundances (with respect to the total density) of sulphur bearing molecules in the CRH model. The destruction of SO_2 at small radii is due to collisional dissociation and leads to the formation of H_2CS, HS and SiS.

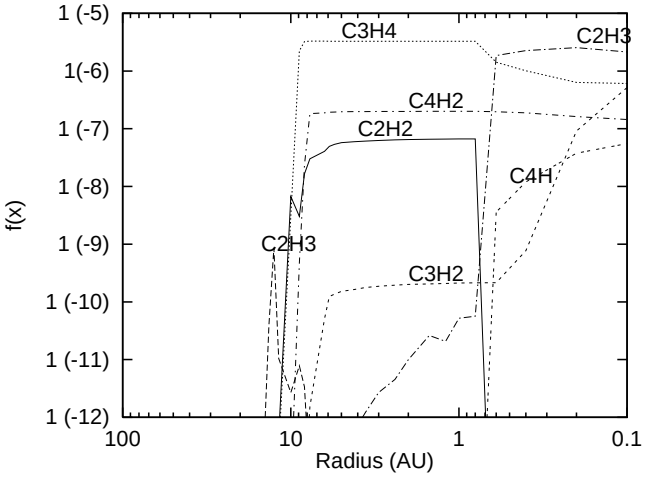

Fig. 4. The radial distribution of the carbon chain molecules with respect to the total density in the CRH model.

Collisional dissociation in the central regions begins to break up the molecules by removing H–atoms and producing unsaturated molecules.

3.6. Nitrogen–bearing species

Ammonia is the dominant form of nitrogen in both models and is formed efficiently on the grains. Other abundant molecules are N_2, HCN, HNC and HC_3N (see Fig. 5). CH_3CN shows considerable variation between the models, being a factor of 10^4 higher in model GR. CH_3CN is formed in the gas by

$$\mathrm{HCN} \stackrel{\mathrm{CH_3^+}}{\longrightarrow} \mathrm{H_4C_2N^+} \stackrel{e}{\longrightarrow} \mathrm{CH_3CN} \qquad (25)$$

and frozen out. In model CRH the abundance is low due to the removal of all molecules from the gas in the outer part of the disk, thus preventing further formation of CH_3CN. In model GR

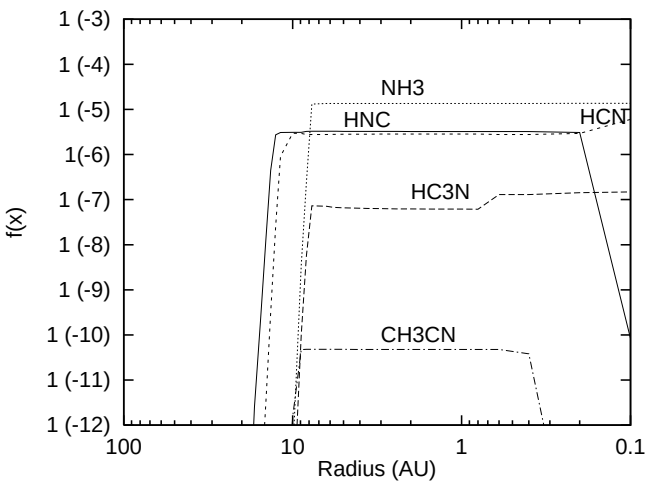

Fig. 5. The fractional abundances with respect to the total hydrogen abundance of the nitrogen–bearing molecules.

the slow return of molecules (in this case especially HCN and CH_4) means that gas phase formation of CH_3CN can continue between 10 and 100 AU. Once formed CH_3CN either freezes out or reacts with H^+ to form $H_4C_2N^+$ which is recycled to CH_3CN.

At very small radii HC_3N and HNC are processed into HCN. All three molecules are destroyed by collisional dissociation but the rate of destruction of HCN is lower. The rate for HCN is measured (Mallard et al. 1994) whereas for the other two species it has been estimated and therefore this conversion may not be real. Assuming for the moment that our rates are not unrealistic CH_3CN and HNC dissociate forming CN which can then react with H_2 to produce HCN. HNC cannot reform since its formation route is via $HCNH^+$.

3.7. The dynamical and chemical timescales

We have assumed that there is a limited period of time for which the physical parameters of the gas remain constant and that this is governed by the rate of diffusion of the gas. If the chemistry is allowed to proceed indefinitely then the results depend on the position in the disk In the outer parts of the disk where thermal desorption can only remove the weakly bound molecules we find that if the chemistry is allowed to run for more than 1 Myrs, the nature of the gas changes, with it becoming depleted of molecules as the lighter species e.g. CO are processed into less volatile molecules and retained on the grain rather than being returned to the gas (Fig. 6. In the case of CO and CH_4, the carbon ends up in solid CO_2, C_3H_4, C_4H_2 and CH_3OH. However as the lifetime of the disk is not expected to greatly exceed 1 Myrs (Strom et al. 1993) this processing would not appear to be important.

At each radius the chemistry reaches a quasi–steady state on a timescale shorter than the diffusive timescale and the abundances do not change much before the diffusive timescale is reached (Fig. 6).

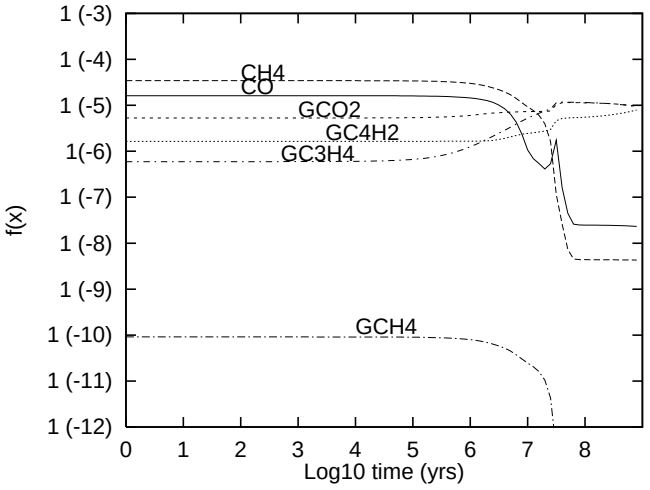

Fig. 6. The time–dependent chemistry at R = 10 AU for a model including desorption due to cosmic ray heating. The abundances shown are fractional with respect to the total density of the gas. At 10 AU the temperature is 55 K and the density is 4.2×10^{12} cm^{-3}. The prefix 'G' indicates that the molecule is in the solid form. The initially high abundance of CO is reduced after 10^6 years as the carbon is incorporated into other, less volatile, molecules which when frozen out are retained on the grain. This can be seen by the increase in the abundance of solid C_3H_4 and C_4H_2. The input to the model at the next radius point is taken at 3×10^4 years, a point at which the abundances are stable.

3.8. The effect of the initial abundances

If the elements are assumed to be initially atomic at 100 AU then the chemistry proceeds quickly (due to the high density) to form more realistic molecules within 0.05 years. If desorption is not included molecules will freezeout on to the grains within 0.2 years.

Limiting the input species to H, H_2, CO, H_2O and N_2 with the other elements assumed to be bound up in the grains (as in Bauer et al. 1997 for example) will severely limit the chemistry. Complex molecules will not form due to the lack of atoms available for reaction at the start of the model and the lack of chemistry which can occur before the temperature has reached sufficiently high values. Hence these input abundances lead to a disk which is dominated by the input molecules until very small radii are reached.

A more realistic alternative to either of the above starting points would seem to be to remember that a protoplanetary disk has evolved out of a molecular cloud and therefore the material from which it is formed is likely to reflect that previous environment. In order to determine whether this would have a significant effect on our results, we have also run our models using the output from a dark cloud model to provide the initial species abundances. We ran the same chemical network for 1 Myrs at a density of 2×10^4 cm^{-3} and a temperature of 10 K. Freezeout and desorption due to cosmic ray heating were included. This resulted in a cloud which consisted of both gaseous and mantle material.

The majority of molecules are unaffected by the choice of input abundances with their calculated abundances varying at most by a factor of 2 – 3. There are some exceptions to this which are summarized below.

1. In model CRH molecular cloud input abundances cause a huge increase in the fractional abundance of CH_3CN from 10^{-10} to 3×10^{-7}, bringing the abundance of this species up to the levels seen in model GR. This is due to the efficient production of CH_3CN in the molecular cloud model by Reaction 25. Some other nitrogen molecules e.g. HNC and HCN are relatively unaffected by the input abundances but NH_3 is reduced. The effect is most pronounced in model GR where the peak fractional abundance falls from 1.4×10^{-5} to 7×10^{-9}. In model CRH the decrease is a factor of 10.
2. The majority of silicon–bearing molecules are unaffected by the choice of input abundances. The two exceptions to this are SiO and SiO_2 which show an increase of a factor of 10 in both models.
3. Oxygen–bearing molecules are most affected in model GR with O_2 now showing a fractional abundance of 10^{-6} between 14 and 1.5 AU. With atomic input abundances the abundance in this region is about 10^{-10}. CH_3OH remains the same in both models but CH_2CO is reduced by a factor of 10 when molecular abundances are used.

We conclude that, with a few exceptions which have been discussed above, the choice of input abundances does not greatly affect our results. Since the relatively large differences between our two input choices do not result in huge differences in the output for the majority of species we can be reasonably confident that the fact that we do not know the exact initial chemical conditions will not alter the main results of our model.

4. Conclusions

The time–dependent chemistry in a protoplanetary disk is investigated between 100 and 0.1 AU. We find that there is a large region of the disk where gas phase chemical reactions are inefficient and the abundances here reflect the values set in the outer parts of the disk. Even with ionization by cosmic rays in the outer part of the disk and by the decay of ^{26}Al in the dense inner parts of the disk, the chemistry is dominated by neutral–neutral reactions with few ions being present. In the innermost part of the disk where the temperature and density are high, collisional dissociation is important although three body reactions have little effect. Even in these regions the temperature is not sufficiently high to destroy the dust (unlike in other models) and ion–molecule chemistry reported by Finocchi et al. (1997) is not seen. This is partly due to the differences in viscosity discussed above. In future models we intend to consider the dust destruction region by extending our computations to smaller radii.

Neither desorption process considered is efficient at keeping material in the gas in the cold outer part of the disk, although explosions triggered by grain–grain collisions can maintain frac-

Table A1. The collisional dissociation and three body reactions used in this model. References are KM81: Kerr & Moss (1981); CBT82: Cherchneff et al. (1982); Baulch92: Baulch et al. (1992); Bahn68: Bahn (1968); NIST: Mallard et al. (1994); R97: Millar et al. (1997). E indicates that the rate has been estimated. The rate is given in the form $\alpha(T/300)^{\beta}exp(-\gamma/T)$.

Number	Reaction	α	β	γ	Reference
1	$C_2 + M \leftrightarrow C + C + M$	6.17e-10	0.00	69823.0	NIST
2	$C_3 + M \leftrightarrow C_2 + C + M$	6.17e-10	0.00	69823.0	E
3	$CH + M \leftrightarrow C + H + M$	3.16e-10	0.00	33700.0	NIST
4	$CH_2 + M \leftrightarrow CH + H + M$	6.64e-09	0.00	41800.0	NIST
5	$CH_2 + M \leftrightarrow H_2 + C + M$	2.16e-10	0.00	29700.0	NIST
6	$CH_3 + M \leftrightarrow CH + H_2 + M$	1.15e-09	0.00	41500.0	NIST
7	$CH_3 + M \leftrightarrow CH_2 + H + M$	1.70e-08	0.00	45600.0	Baulch92
8	$CH_4 + M \rightarrow CH_3 + H + M$	1.20e-06	0.00	47000.0	Baulch92
9	$CH_3 + H + M \rightarrow CH_4 + M$	9.62e-31	-1.80	3231.0	Baulch92
10	$C_2H + M \leftrightarrow C_2 + H + M$	3.74e-10	0.00	50400.0	NIST
11	$C_3H + M \leftrightarrow C_3 + H + M$	1.00e-10	0.00	48600.0	E
12	$C_2H_2 + M \leftrightarrow C_2 + H_2 + M$	7.59e-17	0.00	2069.0	NIST
13	$C_2H_2 + M \leftrightarrow C_2H + H + M$	6.97e-08	0.00	54434.0	CBT92
14	$C_3H_2 + M \leftrightarrow C_3H + H + M$	1.00e-10	0.00	48600.0	E
15	$C_4H_2 + M \leftrightarrow C_4H + H + M$	5.91e-07	0.00	40292.0	NIST
16	$CS + M \leftrightarrow C + S + M$	1.00e-10	0.00	48600.0	E
17	$HCS + M \leftrightarrow H + CS + M$	1.00e-10	0.00	48600.0	E
18	$CN + M \leftrightarrow C + N + M$	3.32e-10	0.00	74989.0	NIST
19	$HCN + M \leftrightarrow H + CN + M$	2.08e-08	0.00	54630.0	NIST
20	$S_2 + M \rightarrow S + S + M$	7.95e-11	0.00	38749.0	NIST
21	$S + S + M \rightarrow S_2 + M$	2.76e-33	-0.50	0.0	CRC
22	$HS + M \leftrightarrow H + S + M$	1.00e-10	0.00	48600.0	E
23	$H_2S + M \leftrightarrow HS + H + M$	7.70e-10	0.00	41500.0	NIST
24	$SO + M \leftrightarrow S + O + M$	6.61e-10	0.00	53885.0	NIST
25	$N_2 + M \rightarrow N + N + M$	9.21e-05	-2.50	113240.0	NIST
26	$N + N + M \rightarrow N_2 + M$	9.53e-34	-0.50	0.0	CRC
27	$NH + M \rightarrow N + H + M$	4.40e-10	0.00	38000.0	NIST
28	$N + H + M \rightarrow NH + M$	3.09e-32	-0.50	0.0	CRC
29	$NH_2 + M \rightarrow NH + H + M$	1.00e-36	0.50	11372.0	Bahn
30	$NH + H + M \rightarrow NH_2 + M$	3.18e-33	-0.50	0.0	Bahn
31	$NH_3 + M \rightarrow NH_2 + H + M$	3.46e-08	0.00	46740.0	NIST
32	$NH_2 + H + M \rightarrow NH_3 + M$	1.32e-33	0.00	4366.0	CRC
33	$NH_3 + M \leftrightarrow NH + H_2 + M$	1.05e-09	0.00	47000.0	NIST
34	$NS + M \leftrightarrow N + S + M$	1.00e-10	0.00	48600.0	NIST
35	$NO + M \rightarrow N + O + M$	4.10e-09	0.00	75380.0	NIST
36	$N + O + M \rightarrow NO + M$	3.86e-34	0.00	2573.0	Bahn
37	$SiH + M \leftrightarrow Si + H + M$	1.00e-10	0.00	48600.0	E
38	$SiH_2 + M \leftrightarrow SiH + H + M$	7.60e-08	-1.80	19219.0	NIST
39	$SiH_3 + M \leftrightarrow SiH + H_2 + M$	4.98e-10	0.00	4534.0	NIST
40	$SiH_4 + M \leftrightarrow SiH_3 + H + M$	1.00e-10	0.00	48600.0	E
41	$SiH_4 + M \leftrightarrow SiH_2 + H_2 + M$	1.00e-10	0.00	48600.0	E
42	$SiC + M \leftrightarrow Si + C + M$	1.00e-10	0.00	48600.0	E
43	$HCSi + M \leftrightarrow H + SiC + M$	1.00e-10	0.00	48600.0	E
44	$SiN + M \leftrightarrow Si + N + M$	1.00e-10	0.00	48600.0	E
45	$HNSi + M \leftrightarrow H + SiN + M$	1.00e-10	0.00	48600.0	E
46	$SiS + M \leftrightarrow Si + S + M$	1.00e-10	0.00	48600.0	E
47	$SiO + M \leftrightarrow Si + O + M$	1.00e-10	0.00	48600.0	E
48	$O_2 + M \rightarrow O + O + M$	5.16e-10	0.00	58410.0	NIST
49	$O + O + M \rightarrow O_2 + M$	5.25e-35	0.00	902.0	CRC
50	$OH + M \rightarrow O + H + M$	4.00e-09	0.00	50000.0	NIST
51	$O + H + M \rightarrow OH + M$	6.32e-34	0.00	1960.0	CRC
52	$H_2O + M \rightarrow OH + H + M$	5.80e-09	0.00	52920.0	Baulch92
53	$OH + H + M \rightarrow H_2O + M$	6.86e-31	-2.00	0.0	NIST
54	$CO + M \rightarrow C + O + M$	1.93e-06	0.00	98700.0	RB
55	$C + O + M \rightarrow CO + M$	2.14e-29	-3.08	2114.0	CRC
56	$CO_2 + M \rightarrow CO + O + M$	8.01e-11	0.00	26900.0	NIST
57	$CO + O + M \rightarrow CO_2 + M$	9.56e-34	0.00	1060.0	CRC

Table A1. (continued)

58	HCO	+	M			→	CO	+	H	+	M	2.39e-10	0.00	8133.0	NIST
59	H	+	CO	+	M	→	HCO	+	M			5.30e-34	0.00	370.0	Baulch92
60	H_2CO	+	M			↔	HCO	+	H	+	M	2.10e-08	0.00	39200.0	NIST
61	H_2CO	+	M			↔	H_2	+	CO	+	M	3.95e-09	0.00	17500.0	NIST
62	C_2H_3	+	M			↔	C_2H_2	+	H	+	M	5.07e-20	-7.50	22900.0	NIST
63	C_3H_4	+	M			↔	C_3H_3	+	H	+	M	1.66e-07	0.00	35226.0	NIST
64	CH_2CO	+	M			↔	CH_2	+	CO	+	M	5.97e-09	0.00	29828.0	NIST
65	CH_3OH	+	M			↔	CH_3	+	OH	+	M	3.32e-07	0.00	34399.0	NIST
66	OCS	+	M			↔	CO	+	S	+	M	4.82e-10	0.00	32000.0	NIST
67	SO_2	+	M			→	SO	+	O	+	M	6.60e-09	0.00	50517.0	NIST
68	SO	+	O	+	M	→	SO_2	+	M			1.86e-31	-0.50	0.0	CRC
69	H_2CS	+	M			↔	HCS	+	H	+	M	1.00e-10	0.00	48600.0	E
70	C_4H	+	M			↔	C_4	+	H	+	M	1.00e-10	0.00	48600.0	E
71	C_3H_3	+	M			↔	C_3H_2	+	H	+	M	1.00e-10	0.00	48600.0	E
72	C_2S	+	M			↔	C_2	+	S	+	M	1.00e-10	0.00	48600.0	E
73	C_2S	+	M			↔	CS	+	C	+	M	1.00e-10	0.00	48600.0	E
74	C_2H_3	+	M			↔	C_2H_2	+	H	+	M	1.00e-10	0.00	48600.0	E
75	C_4	+	M			↔	C_3	+	C	+	M	1.00e-10	0.00	48600.0	E
76	C_3S	+	M			↔	C_3	+	S	+	M	1.00e-10	0.00	48600.0	E
77	C_3S	+	M			↔	CS	+	C_2	+	M	1.00e-10	0.00	48600.0	E
78	SiO_2	+	M			↔	SiO	+	O	+	M	1.00e-10	0.00	48600.0	E
79	HNC	+	M			↔	CN	+	H	+	M	1.00e-10	0.00	48600.0	E
80	HC_3N	+	M			↔	C_3N	+	H	+	M	1.00e-10	0.00	48600.0	E
81	C_3O	+	M			↔	C_2	+	CO	+	M	1.00e-10	0.00	48600.0	E
82	SiH_2	+	M			↔	Si	+	H_2	+	M	7.60e-08	-1.76	19219.0	MICK
83	C_3N	+	M			↔	C_2	+	CN	+	M	1.00e-10	0.00	48600.0	E
84	CH_3CN	+	M			↔	CH_3	+	CN	+	M	1.00e-10	0.00	48600.0	E
85	H	+	H	+	H_2	→	H_2	+	H_2			8.72e-33	-0.60	0.0	CBT92
86	H_2	+	H_2			→	H	+	H	+	H_2	1.50e-09	0.00	46350.0	R97
87	H	+	H	+	H	→	H_2	+	H			1.83e-31	-1.00	0.0	CBT92
88	H_2	+	H			→	H	+	H	+	H	3.75e-08	-0.50	53280.0	R97

tional abundances between 10^{-10} and 10^{-8} for some molecules. The two models produce very similar results for most molecules but CH_3CN is a factor of 4000 higher in model GR and may therefore one day provide an observational test of desorption efficiency in these regions. The results are found to be unaffected by the choice of initial chemical abundances, with only a few species e.g. CH_3CN, NH_3, SiO, SiO_2 and CH_2CO being greatly affected. Hence the exact composition of the molecular cloud when the disk forms will not greatly alter the composition of the disk.

Acknowledgements. Astrophysics at UMIST is supported by PPARC. This research was partially supported by a British Council/DAAD grant to KW and TH and by the DFG grant He 1935/5–2 within the programme 'Physics of star formation'.

Appendix A: collisional dissociation and three body reaction rates, see Table A1 on last page

References

Aikawa, Y., Umebayashi, T., Nakano, T., 1997, ApJ 486, L51
Bahn, G. S., 1968, Reaction rate compilations for the H–O–N system, Gordon & Breach, New York.
Bauer, I., Finocchi, F., Duschl, W. J., Gail, H.–P., Schlöder, J. P., 1997, A&A 317, 273
Baulch, D. L., Cobos, E. J., Cox, R. A., Esser, C., Franck, P., Just, Th., Kerr, J. A., Piling, M. J., Troe, J., Walker, R. W., Warnatz, J., 1992, J. Phys. Chem. Ref. Data 21, 411
Beckwith, S. V. W., Sargent, A. I., 1993, in: Protostars and Planets III, eds. E. H. Levy, J. I. Lunine, University of Arizona Press, Tucson, p. 521
Bell, K. R., Lin, D. N. C., 1994, ApJ 427, 987
Bell, K. R., Cassen, P. M., Klahr, H. H., Henning, Th., 1997, ApJ 486, 372
Bergin, E. A., Langer, W. D., 1997, ApJ 486, 316
Blake, G. A., van Dishoeck, E. F., Sargent, A. I., 1992, ApJ 391, L99
Bodenheimer, P., 1995, ARA&A 33, 199
Chase, M. W., Davies, C. A., Downet, J. R., Frurip, D. J., McDonald, R. A., Syverud, A. N., 1985, J. Phys. Chem. Ref. Data 14, Suppl. 1, 1
Duschl, W. J., Gail, H.–P., Tscharnuter, W. M., 1996, A&A 312, 624
Dutrey, A., Guilloteau, S., Guélin, M., 1997, A&A 317, L55
Finocchi, F., Gail, H.–P., Duschl, W. J., 1997, A&A 325, 1264
Hasegawa, T. I., Herbst, E., 1993, MNRAS 261, 83
Henning, Th., Stognienko, R., 1996, A&A 311, 291
Kerr, J. A., Moss, S. J., 1981, CRC Handbook of bimolecular and termolecular gas reactions Vol 2, CRC Press Inc.
Kippenhahn, R., Weigert, A., Hofmeister E., 1967, Methods in computational physics 7, 129

Léger, A., Jura, M., Omont, A., 1985, A&A 144, 147
Levermore, C. D., Pomraning, G. C., 1981, ApJ 262, 768
Mallard, W. G., Westley, F., Herron, J. T., Hampson, R. F., Frizzell, D. H., 1994, NIST Chemical Kinetics Database Version 6.0, National Institute of Standards and Technology, Gaithersburg (MD)
Meyer, F., Meyer–Hofmeister, E., 1981, A&A 104, L10
Meyer, F., Meyer–Hofmeister, E., 1982, A&A 106, 34
Millar, T. J., Farquhar, P. R. A., Willacy, K., 1997, A&AS 121, 139
Ossenkopf, V., 1993, A&A 280, 617
Pringle, J. E., 1981, ARA&A 19, 137
Różycka, M. N., Bodenheimer, P. H., Bell, K. R., 1994, ApJ 423, 736
Sandford, S., Allamandola, L. J., 1993, ApJ 417, 815
Schutte, W. A., Greenberg, J. M., 1991, A&A 244, 190
Shakura, N. I., Sunyaev, R. A., 1973, A&A 24, 337
Shalabeia, O., Greenberg, J. M, 1994, A&A 290, 266
Strom, S. E., Edwards, S., Skrutskie, M. F., 1993, in: Protostars and Planets III, eds. E. H. Levy, J. I. Lunine, University of Arizona Press, Tucson, p. 837
Taylor, S., Williams, D. A., Bennett, A., 1991, MNRAS 248, 148
Umebayashi, T., Nakano, T., 1981, PASJ 33, 617
Willacy, K., Millar, T. J., 1998, MNRAS 298, 562
Yamamoto, T., 1991, in: Comets in the Post–Halley Era, eds. Newburn R. L. Jr. et al., Kluwer Academic Publishers, p. 361
Yamamoto, T., Nakagawa, N., Fukui, Y., 1983, A&A 122, 171